Transmission of dipole radiation through interfaces and the phenomenon of anti-critical angles

Henk F. Arnoldus and John T. Foley

Department of Physics and Astronomy, Mississippi State University, P.O. Drawer 5167, Mississippi State, Mississippi 39762-5167

Received August 18, 2003; revised manuscript received December 8, 2003; accepted January 21, 2004

Radiation emitted by an electric dipole consists of traveling and evanescent plane waves. Usually, only the traveling waves are observable by a measurement in the far field, since the evanescent waves die out over a length of approximately a wavelength from the source. We show that when the radiation is passed through an interface with a medium with an index of refraction larger than the index of refraction of the embedding medium of the dipole, a portion of the evanescent waves are converted into traveling waves, and they become observable in the far field. The same conclusion holds when the waves pass through a layer of finite thickness. Waves that are transmitted under an angle larger than the so-called anti-critical angle $\theta_{\mathrm{ac}}^{(1)}$ are shown to originate in evanescent dipole waves. In this fashion, part of the evanescent spectrum of the radiation becomes amenable to observation in the far field. We also show that in many situations the power in the far field coming from evanescent waves greatly exceeds the power originating in traveling waves.

OCIS codes: 240.0240, 260.2110.

1. INTRODUCTION

When a monochromatic plane wave, traveling in a medium with index of refraction n_1, is incident on a planar interface with a medium of index of refraction $n_2 < n_1$, then the transmitted wave will be evanescent (exponentially decaying away from the surface) when the angle of incidence exceeds the critical angle θ_c. For later reference we indicate this angle by $\theta_c^{(2)}$, and it is given by

$$\sin \theta_c^{(2)} = n_2/n_1. \tag{1}$$

If this transmitted wave encounters a second interface parallel to the first, with a medium of index of refraction n_3, then the wave can emerge as either traveling or evanescent. For instance, if $n_3 > n_1$, then the wave transmitted through the layer will be traveling again.

Another example of the occurrence of a critical angle is when we consider only the waves in medium n_1 and medium n_3 but with a layer of medium n_2 in between. If $n_3 < n_1$, then there exists another critical angle $\theta_c^{(1)}$:

$$\sin \theta_c^{(1)} = n_3/n_1. \tag{2}$$

When the angle of incidence of the wave in medium n_1 exceeds the critical angle $\theta_c^{(1)}$, then the emerging wave in medium n_3 is evanescent, no matter the character of the wave in the layer in between. In any case, upon transmission through an interface or a layer, a traveling wave can be converted into an evanescent wave, and vice versa.

Usually, an incident wave is traveling. However, in the established research on near-field optics it has become evident that evanescent waves play a crucial role.[1–7] In a scanning near-field microscope a probe, consisting of a fiber tip, is moved over a nanosized sample. The probe can either emit light for illumination of the sample (emission mode) or collect light scattered by the sample (collection mode). In the emission mode, the light coming out of the fiber tip contains evanescent waves that are produced by diffraction through the small aperture (the opening of the tip),[8–10] and in the collection mode, the modes of the fiber couple to the evanescent modes of the scattered light. In a different configuration, a sample can be illuminated by either a traveling or an evanescent wave, generated by total internal reflection, and the scattered field or the fluorescence (in case of a molecule) is observed by a macroscopic detector in the far field. In this case, the sample is positioned on an oil-immersion hemispherical lens. Traveling waves from the field scattered by the sample exit the lens under an angle of at most the critical angle for total internal reflection, given by Eq. (1), and this radiation is sometimes called "allowed light." It has long been recognized,[11–15] however, that if one seeks to improve the resolution of such an imaging device into the nanometer region, then also the waves that appear under an angle larger than the critical angle have to be observed. Since this radiation has its origin in scattered evanescent waves, this radiation is given the name "forbidden light."[16]

Of particular interest is the radiation emitted by an electric dipole located in the vicinity of a surface, since such radiation is emitted by atoms and molecules as fluorescence. This radiation is a superposition of traveling and evanescent waves. Normally, the traveling waves are detected in the far field with a macroscopic device such as a photomultiplier, but since evanescent waves can be transformed into traveling waves at an interface, it should be possible to detect traveling waves in the far field that have their origin in evanescent dipole waves.[17] These waves appear as forbidden light under an angle larger than the critical angle for total internal reflection, and this radiation has been indeed observed for dipole radiation.[18]

We shall consider the situation shown in Fig. 1, where the dipole $\mathbf{d}$ is located on the z axis at a distance H above the first interface, which is the xy plane. The second boundary is at $z = -L$, and the indices of refraction are n_1, n_2, and n_3, assumed to be positive. The dipole, embedded in medium n_1, oscillates harmonically as $\mathbf{d}(t) = \mathrm{Re}[\mathbf{d}\exp(-i\omega t)]$. Without boundaries, the complex amplitude $\mathbf{E}_s(\mathbf{r})$ of the dipole (source) field $\mathbf{E}_s(\mathbf{r}, t) = \mathrm{Re}[\mathbf{E}_s(\mathbf{r})\exp(-i\omega t)]$ can be represented as an angular spectrum, according to[19–21]

$$\mathbf{E}_s(\mathbf{r}) = \frac{i}{8\pi^2\epsilon_o n_1^2}\int \mathrm{d}^2\mathbf{k}_\parallel \frac{1}{\beta}[k_o^2 n_1^2 \mathbf{d} - (\mathbf{d}\cdot\mathbf{k})\mathbf{k}] \times \exp[i\mathbf{k}\cdot(\mathbf{r} - H\mathbf{e}_z)], \qquad z \neq H, \tag{3}$$

with $k_o = \omega/c$. This is a superposition of plane waves with wave vectors $\mathbf{k} = \mathbf{k}_\parallel + \beta\,\mathrm{sgn}(z - H)\mathbf{e}_z$, and here $\mathbf{k}_\parallel$ indicates the component of $\mathbf{k}$ parallel to the xy plane. The integration then runs over the entire $\mathbf{k}_\parallel$ plane. The parameter β, which is the z component of $\mathbf{k}$ for $z > H$ and the negative of the z component of $\mathbf{k}$ for $z < H$, is defined as

$$\beta = \begin{cases} \sqrt{k_o^2 n_1^2 - k_\parallel^2} & \text{for } k_\parallel < k_o n_1 \\ i\sqrt{k_\parallel^2 - k_o^2 n_1^2} & \text{for } k_\parallel > k_o n_1 \end{cases}. \tag{4}$$

For $k_\parallel < k_o n_1$, β is real, and the corresponding wave is a traveling wave. On the other hand, when $k_\parallel > k_o n_1$, β is positive imaginary, representing an evanescent wave that decays exponentially away from the plane $z = H$ on both sides. The corresponding magnetic field is given by

$$\mathbf{B}_s(\mathbf{r}) = -\frac{i}{\omega}\nabla \times \mathbf{E}_s(\mathbf{r}), \tag{5}$$

and it can be verified by inspection that the individual waves satisfy the source-free Maxwell equations for $z > H$ and $z < H$. These partial waves then serve as the incident field on the boundary with the xy plane, giving rise to reflection and transmission.

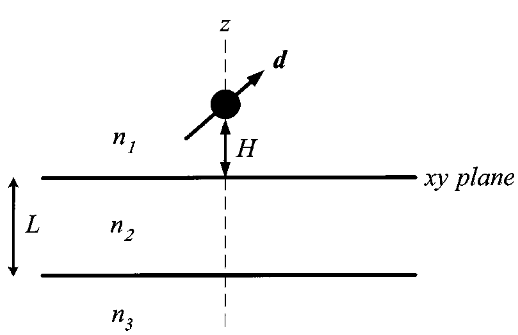

Fig. 1. An electric dipole, with dipole moment $\mathbf{d}$, in a medium with index of refraction n_1 is located a distance H above the xy plane and on the z axis. The region $-L < z < 0$ contains a dielectric material with index of refraction n_2, and the region $z < -L$ is filled with a material with index of refraction n_3.

2. WAVE VECTORS AND POLARIZATION CONVENTION

For a given incident plane wave with wave vector $\mathbf{k}$, the resulting reflected and transmitted waves are again plane waves. Figure 2 shows the various wave vectors, including the decay direction in the case that the wave is evanescent. Boundary conditions at $z = 0$ and $z = -L$ require that all waves have the same parallel component $\mathbf{k}_\parallel$. It will be convenient to introduce a dimensionless variable for the magnitude of $\mathbf{k}_\parallel$ by

$$\alpha = k_\parallel / k_o. \tag{6}$$

If the incident wave is traveling, with an angle of incidence θ_{inc}, we have $\alpha = n_1 \sin\theta_{\mathrm{inc}}$. For a wave with wave vector $\mathbf{k}_a$ ($a = r$ for the reflected wave, t for transmitted, etc.) in medium n_i, the wave number is $k_a = k_o n_i$, and since the parallel part of the wave vector is determined by the incident field, we have for the z component $k_{a,z} = \pm k_o(n_i^2 - \alpha^2)^{1/2}$, leaving only the sign to be determined. We furthermore introduce the abbreviation

$$\nu_i = \sqrt{n_i^2 - \alpha^2}, \qquad i = 1, 2, 3, \tag{7}$$

and it is understood that we take ν_i to be positive imaginary when $\alpha > n_i$. Parameter β from Eq. (4) then becomes $\beta = k_o\nu_1$, so that a wave vector of the source field is

$$\mathbf{k} = \begin{cases} \mathbf{k}_\parallel + k_o\nu_1\mathbf{e}_z, & z > H \\ \mathbf{k}_\parallel - k_o\nu_1\mathbf{e}_z, & z < H \end{cases}. \tag{8}$$

The specular (reflected) wave has a wave vector

$$\mathbf{k}_r = \mathbf{k}_\parallel + k_o\nu_1\mathbf{e}_z \tag{9}$$

corresponding to a wave traveling in the positive z direction ($\alpha < n_1$) or decaying away from the xy plane ($\alpha > n_1$). For the two waves in the layer, we have $\mathbf{k}_\pm = \mathbf{k}_\parallel \pm k_o\nu_2\mathbf{e}_z$ corresponding to waves that travel or decay, as shown in Fig. 2. The transmitted wave travels or decays in the negative z direction, and therefore its wave vector is

$$\mathbf{k}_t = \mathbf{k}_\parallel - k_o\nu_3\mathbf{e}_z. \tag{10}$$

The most convenient way to calculate the reflected and transmitted fields is by first decomposing the partial waves of the source field into s- and p-polarized waves.[22,23] Given $\mathbf{k}_\parallel$, we define the unit vector for s polarization by

$$\mathbf{e}_s = \frac{1}{k_\parallel}\mathbf{k}_\parallel \times \mathbf{e}_z, \tag{11}$$

which is the same for all waves. For p polarization we take

$$\mathbf{e}_{p,a} = \frac{1}{k_a}\mathbf{k}_a \times \mathbf{e}_s, \tag{12}$$

which depends on the corresponding wave vector $\mathbf{k}_a$. For instance, for the t wave we have

$$\mathbf{e}_{p,t} = -\frac{1}{n_3}[\nu_3(\mathbf{k}_\parallel/k_\parallel) + \alpha\mathbf{e}_z]. \tag{13}$$

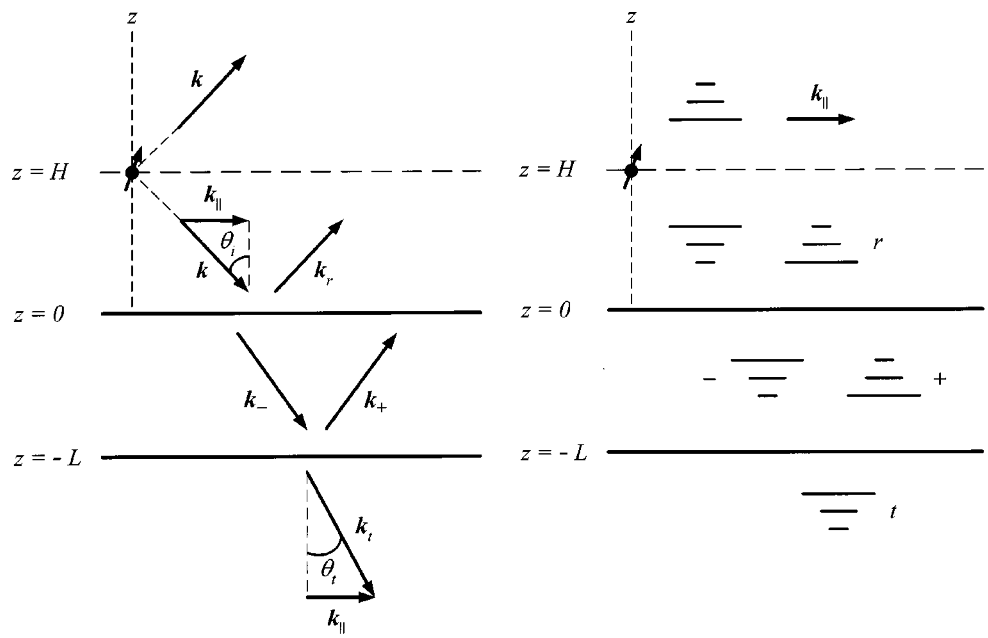

Fig. 2. Angular spectrum source (dipole) waves with wave vectors $\mathbf{k}$ emanate from the plane $z = H$. (a) A traveling dipole wave, for $z > H$, travels in the positive z direction and for $z < H$ in the negative z direction. When the dipole wave is traveling, so is the specular wave, represented by wave vector $\mathbf{k}_r$. (b) An evanescent dipole wave decays in the positive z direction for $z > H$ and in the negative z direction for $z < H$. In this case, the reflected wave (r) is also evanescent, and each wave travels along the xy plane with wave vector $\mathbf{k}_\parallel$. The waves in the layer can be either traveling or evanescent, and also the transmitted wave can be either traveling or evanescent, traveling or decaying away from the boundary $z = -L$.

It should be noted that for evanescent waves the z component of $\mathbf{k}_a$ is imaginary, and therefore the parallel component of $\mathbf{e}_{p,a}$ becomes imaginary.

3. FIELDS IN VARIOUS REGIONS

The source field, Eq. (3), for $z < H$ is the incident field on the surface $z = 0$. With the identity

$$k_o{}^2 n_1{}^2 \mathbf{d} - (\mathbf{d}\cdot\mathbf{k})\mathbf{k} = k_o{}^2 n_1{}^2 \sum_{\sigma=s,p} (\mathbf{d}\cdot\mathbf{e}_\sigma)\mathbf{e}_\sigma, \quad (14)$$

we can write each partial wave as a sum of an s-polarized and a p-polarized wave:

$$\mathbf{E}_s(\mathbf{r}) = \frac{ik_o}{8\pi^2\epsilon_o}\int \mathrm{d}^2\mathbf{k}_\parallel \sum_{\sigma=s,p}\frac{\exp(i\nu_1 h)}{\nu_1}(\mathbf{d}\cdot\mathbf{e}_\sigma)\mathbf{e}_\sigma \times \exp(i\mathbf{k}\cdot\mathbf{r}), \qquad z < H. \quad (15)$$

Here we have set $h = k_o H$ for the dimensionless parameter representing the distance between the dipole and the surface. The polarization vectors $\mathbf{e}_\sigma$ follow from the previous section, and they are associated with wave vector $\mathbf{k} = \mathbf{k}_\parallel - k_o\nu_1\mathbf{e}_z$. For $z > H$, vector $\mathbf{k}$ is the same as the wave vector for the specular wave, e.g., $\mathbf{k} = \mathbf{k}_r = \mathbf{k}_\parallel + k_o\nu_1\mathbf{e}_z$, and the source field is

$$\mathbf{E}_s(\mathbf{r}) = \frac{ik_o}{8\pi^2\epsilon_o}\int \mathrm{d}^2\mathbf{k}_\parallel \sum_{\sigma=s,p}\frac{\exp(-i\nu_1 h)}{\nu_1}(\mathbf{d}\cdot\mathbf{e}_{\sigma,r})e_{\sigma,r} \times \exp(i\mathbf{k}_r\cdot\mathbf{r}), \qquad z > H. \quad (16)$$

Each incident partial wave in Eq. (15) couples to a set of waves as shown in Fig. 2. The amplitudes of the remaining waves can be expressed in terms of Fresnel coefficients that determine the amplitude of each wave with respect to the amplitude of the corresponding partial incident wave. For the reflected wave we then obtain

$$\mathbf{E}_r(\mathbf{r}) = \frac{ik_o}{8\pi^2\epsilon_o}\int \mathrm{d}^2\mathbf{k}_\parallel \sum_{\sigma=s,p}\frac{\exp(i\nu_1 h)}{\nu_1}R_\sigma(\alpha) \times (\mathbf{d}\cdot\mathbf{e}_\sigma)\mathbf{e}_{\sigma,r}\exp(i\mathbf{k}_r\cdot\mathbf{r}), \qquad z > 0, \quad (17)$$

with $R_\sigma(\alpha)$ the Fresnel reflection coefficients for s-polarized and p-polarized waves. The Fresnel coefficients can be obtained in the usual way by applying the boundary conditions at $z = 0$ and $z = -L$ for a given incident partial wave. For reference, we have listed these in Appendix A for the configuration shown in Fig. 2. The total field in $z > H$ is then the sum of Eqs. (16) and (17). We write this as

$$\mathbf{E}(\mathbf{r}) = \frac{ik_o}{8\pi^2\epsilon_o}\int \mathrm{d}^2\mathbf{k}_\parallel \frac{1}{\nu_1}\exp[i(\mathbf{k}_\parallel\cdot\mathbf{r} + \nu_1 k_o z)] \times \sum_{\sigma=s,p}[\exp(-i\nu_1 h)\mathbf{d}\cdot\mathbf{e}_{\sigma,r} + \exp(i\nu_1 h)R_\sigma(\alpha)\mathbf{d}\cdot\mathbf{e}_\sigma], \qquad z > H. \quad (18)$$

The field in the region $0 < z < H$ is the sum of Eqs. (15) and (17), and the field in the layer $-L < z < 0$ can be constructed by using the appropriate Fresnel coefficients. We shall omit the explicit expressions here. The transmitted field in the region $z < -L$ can be expressed as

$$\mathbf{E}(\mathbf{r}) = \frac{ik_o}{8\pi^2\epsilon_o}\int \mathrm{d}^2\mathbf{k}_\parallel \frac{1}{\nu_1}\exp[i(\mathbf{k}_\parallel \cdot \mathbf{r} - \nu_3 k_o z + \nu_1 h)] \times \sum_{\sigma=s,\,p} T_\sigma(\alpha)(\mathbf{d}\cdot\mathbf{e}_\sigma)\mathbf{e}_{\sigma,t}, \qquad z < -L, \tag{19}$$

with $T_\sigma(\alpha)$ the Fresnel transmission coefficients.

4. ASYMPTOTIC APPROXIMATION

The radiation is detected at a field point with spherical coordinates $(r,\ \theta,\ \phi)$ and with r large (far field). From Eqs. (18) and (19) we can derive the far-field approximations for the fields in $z > H$ and $z < -L$, respectively, with the method of stationary phase.[24–26] Both expressions are integrals over $\mathbf{k}_\parallel$. In the method of stationary phase it is asserted that the major contribution for r large and θ and ϕ fixed comes from the neighborhood of a point in the $\mathbf{k}_\parallel$ plane, say, $\mathbf{k}_{\parallel,o}$, where the phase is stationary. For an arbitrary function $f(\mathbf{k}_\parallel)$ we then obtain the asymptotic approximation

$$\int \mathrm{d}^2\mathbf{k}_\parallel \frac{1}{k_o\nu_i} f(\mathbf{k}_\parallel)\exp[i(\mathbf{k}_\parallel\cdot\mathbf{r} + k_o\nu_i|z|)] \approx -\frac{2\pi i}{r} f(\mathbf{k}_{\parallel,o})\exp(in_i k_o r), \qquad i = 1 \text{ or } 3, \tag{20}$$

with ν_i given by Eq. (7) and $\mathbf{k}_{\parallel,o} = k_o n_i \sin\theta\,\mathbf{e}_\rho$. Vector $\mathbf{e}_\rho$ is the radial unit vector in the xy plane corresponding to the direction of $\hat{\mathbf{r}}$, e.g., $\mathbf{e}_\rho = \mathbf{e}_x\cos\phi + \mathbf{e}_y\sin\phi$. The magnitude of $\mathbf{k}_{\parallel,o}$ is $k_{\parallel,o} = k_o n_i \sin\theta$, and since in medium n_i we have $\nu_i = n_i|\cos\theta|$, we see that the z component of the corresponding traveling plane wave equals $k_o n_i \cos\theta$. The wave vector of this partial wave in the angular spectrum is therefore $k_o n_i \hat{\mathbf{r}}$. This yields the clear interpretation that the main contribution to the field comes from the traveling plane wave that travels exactly in the direction $\hat{\mathbf{r}}$ of the detector.

The far-field approximation to Eq. (18) is found to be

$$\begin{aligned}\mathbf{E}(\mathbf{r}) = {} & \frac{k_o^2}{4\pi\epsilon_o r}\exp[in_1(k_o r - h\cos\theta)] \times [(\mathbf{d}\cdot\mathbf{e}_\phi)e_\phi + (\mathbf{d}\cdot\mathbf{e}_\theta)e_\theta] \\ & + \frac{k_o^2}{4\pi\epsilon_o r}\exp[in_1(k_o r + h\cos\theta)][R_s(\alpha_o) \\ & \times (\mathbf{d}\cdot\mathbf{e}_\phi)\mathbf{e}_\phi - R_p(\alpha_o)(\mathbf{d}\cdot\mathbf{e}_\theta + 2\sin\theta\,\mathbf{d}\cdot\mathbf{e}_z)\mathbf{e}_\theta],\end{aligned} \tag{21}$$

in terms of the spherical unit vectors $\mathbf{e}_\phi$ and $\mathbf{e}_\theta$. We shall write an equal sign instead of $\approx$. The Fresnel reflection coefficients have to be evaluated at the value of α at the critical point, which is $\alpha_o = k_{\parallel,o}/k_o = n_1\sin\theta$. The first term on the right-hand side is the source wave, which travels directly from the dipole toward the detector, and the second term is the reflected wave. The difference in travel distance is seen to be $2H\cos\theta$, indicating that the reflected wave seems to come from a mirror image of the dipole at a distance H below the interface $z = 0$ and on the z axis. This is even clearer if we write the part with the reflection coefficients as

$$\begin{aligned} & R_s(\alpha_o)(\mathbf{d}\cdot\mathbf{e}_\phi)\mathbf{e}_\phi - R_p(\alpha_o)(\mathbf{d}\cdot\mathbf{e}_\theta + 2\sin\theta\,\mathbf{d}\cdot\mathbf{e}_z)\mathbf{e}_\theta \\ & \quad = -R_s(\alpha_o)(\tilde{\mathbf{d}}\cdot\mathbf{e}_\phi)\mathbf{e}_\phi + R_p(\alpha_o)(\tilde{\mathbf{d}}\cdot\mathbf{e}_\theta)\mathbf{e}_\theta,\end{aligned} \tag{22}$$

where the mirror dipole $\tilde{\mathbf{d}}$ is defined as

$$\tilde{\mathbf{d}} = \mathbf{d}_\perp - \mathbf{d}_\parallel, \tag{23}$$

given that $\mathbf{d} = \mathbf{d}_\perp + \mathbf{d}_\parallel$. In the case of a perfectly conducting substrate, we would have $R_s = -1$ and $R_p = 1$ for every angle of incidence, showing even more the resemblance to the source term.

For the transmitted field we find the asymptotic approximation to be [from Eq. (19)]

$$\begin{aligned}\mathbf{E}(\mathbf{r}) = {} & -\frac{k_o^2 n_3\cos\theta}{4\pi\epsilon_o r}\exp[i(k_o n_3 r + h\nu_{1,o})]\frac{1}{\nu_{1,o}} \\ & \times \Bigg[T_s(\alpha_o)(\mathbf{d}\cdot\mathbf{e}_\phi)\mathbf{e}_\phi - \frac{1}{n_1}T_p(\alpha_o) \\ & \times (\nu_{1,o}\mathbf{d}\cdot\mathbf{e}_\rho + n_3\sin\theta\,\mathbf{d}\cdot\mathbf{e}_z)\mathbf{e}_\theta\Bigg].\end{aligned} \tag{24}$$

Here the value of α in the critical point is $\alpha_o = n_3\sin\theta$, and the Fresnel transmission coefficients have to be evaluated at this α_o. Also, the parameter ν_1 at the critical point appears in this result:

$$\nu_{1,o} = \sqrt{n_1^2 - n_3^2\sin\theta}. \tag{25}$$

It seems that for certain θ, the factor $1/\nu_{1,o}$ in Eq. (24) could present a problem. However, the transmission coefficients $T_\sigma(\alpha)$ are proportional to ν_1 [Eqs. (A5) and (A6)], and therefore the $1/\nu_{1,o}$ in Eq. (24) cancels exactly.

5. INTENSITY DISTRIBUTION

The magnetic field for r large can be obtained from Eqs. (21) and (24) by taking the curl, as in Eq. (5), although it appears easier to take the curl in Eqs. (18) and (19), and then make the asymptotic approximations for the resulting angular spectrum representations of the magnetic field. We thus obtain the relation

$$\mathbf{B}(\mathbf{r}) = \frac{n_i}{c}\hat{\mathbf{r}}\times\mathbf{E}(\mathbf{r}), \qquad i = 1 \text{ or } 3. \tag{26}$$

The Poynting vector

$$\mathbf{S}(\mathbf{r}) = \frac{1}{2\mu_o}\mathrm{Re}\,\mathbf{E}(\mathbf{r})\times\mathbf{B}(\mathbf{r})^*, \tag{27}$$

and the power per unit solid angle, $\mathrm{d}P/\mathrm{d}\Omega = r^2\mathbf{S}(\mathbf{r})\cdot\hat{\mathbf{r}}$, can then be evaluated for the far field with the results from Section 4.

For the dipole moment we write $\mathbf{d} = \mathbf{u}d$, with d complex and the unit vector $\mathbf{u}$ normalized as $\mathbf{u}\cdot\mathbf{u}^* = 1$. The intensity distribution will be normalized as

$$\frac{\mathrm{d}P}{\mathrm{d}\Omega} = P_o A(\theta,\ \phi), \tag{28}$$

with

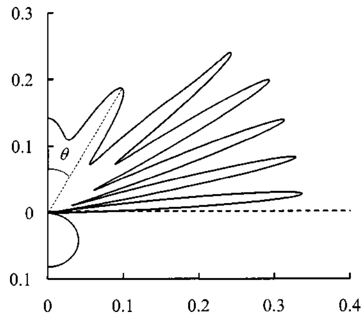

Fig. 3. Polar diagram of the intensity distribution $A(\theta,\ \phi)$. The dashed line indicates the xy plane, and the vertical axis is the z axis. The graph represents $A(\theta,\ \phi)$ as the distance to the origin, given the polar angle θ. The parameters are $n_1 = 1.41$, $n_2 = n_3 = 1$, and $h = 4\pi$. The orientation of the dipole is taken as the spherical unit vector $e_1 = -(\mathbf{e}_x + i\mathbf{e}_y)/\sqrt{2}$, representing a dipole with a dipole moment that rotates counterclockwise in the xy plane. For this case, $A(\theta,\ \phi)$ has no ϕ dependence.

$$P_o = \frac{\omega^4}{12\pi\epsilon_o c^3}\mathbf{d}\cdot\mathbf{d}^*. \tag{29}$$

This P_o is the power radiated by a dipole $\mathbf{d}$ in free space.[27] For $z > H$ we then find

$$A(\theta,\ \phi) = \frac{3n_1}{8\pi}|\mathbf{e}_\theta\cdot\mathbf{u} + \mathbf{e}_\theta\cdot\tilde{\mathbf{u}}R_p(n_1\sin\theta) \times \exp(2in_1h\cos\theta)|^2 + \frac{3n_1}{8\pi}|\mathbf{e}_\phi\cdot\mathbf{u} \times [1 + R_s(n_1\sin\theta)\exp(2in_1h\cos\theta)]|^2, \tag{30}$$

where $\tilde{\mathbf{u}} = \mathbf{u}_\perp - \mathbf{u}_\parallel$, and for $z < -L$ we obtain

$$A(\theta,\ \phi) = \frac{3n_3^3}{8\pi}\cos^2\theta\left[\left|\frac{T_s(n_3\sin\theta)}{\nu_{1,o}}\right|^2|\mathbf{e}_\phi\cdot\mathbf{u}|^2 + \frac{1}{n_1^2}\left|\frac{T_p(n_3\sin\theta)}{\nu_{1,o}}\right|^2 \times|\nu_{1,o}\mathbf{u}\cdot\mathbf{e}_\rho + n_3\sin\theta\,\mathbf{u}\cdot\mathbf{e}_z|^2\right] \times\exp[-2h\,\mathrm{Im}(n_1^2 - n_3^2\sin^2\theta)^{1/2}]. \tag{31}$$

A typical intensity distribution pattern is shown in Fig. 3. It shows the familiar lobe structure in $z > H$, which is due to interference between the waves emitted directly by the dipole and the reflected waves.[28–31] In the region $z < -L$, there is not such a structure since there is no interference in this region. A similar result was derived in Ref. 18 for a single interface.

6. ANTI-CRITICAL ANGLE OF THE FIRST KIND

It follows from the method of stationary phase that for a given observation direction $\hat{\mathbf{r}}$, effectively only one partial wave of the angular spectrum contributes to the emitted power in that direction. This wave has wave vector $k_on_1\hat{\mathbf{r}}$ for an observation point in $z > H$ and $k_on_3\hat{\mathbf{r}}$ for detection in $z < -L$. Since each wave in Fig. 2(a) has the same $\mathbf{k}_\parallel$, and thereby the same α, we see that $\alpha = n_1\sin\theta_{\mathrm{inc}} = n_3\sin\theta_t$, relating the angle of incidence θ_{inc} and the angle of transmission θ_t. For detection in $z < -L$, angle θ_t is in the range $0 \leqslant \theta_t < \pi/2$. Given θ_t, the angle of incidence follows from $\sin\theta_{\mathrm{inc}} = (n_3/n_1)\sin\theta_t$. But if $n_3 > n_1$, this equation does not necessarily have a solution. Apparently, there exists a transmission angle $\theta_{\mathrm{ac}}^{(1)}$, given by

$$\sin\theta_{\mathrm{ac}}^{(1)} = n_1/n_3, \tag{32}$$

which has the significance that if $\theta_{\mathrm{ac}}^{(1)} < \theta_t < \pi/2$, there is no corresponding θ_{inc}. However, there is a corresponding α and therefore a corresponding incident wave. For $\theta_{\mathrm{ac}}^{(1)} < \theta_t < \pi/2$, the values of α are in the range $n_1 < \alpha < n_3$, since $\alpha = n_3\sin\theta_t$, and this is in the evanescent region of the angular spectrum of the dipole. Consequently, any radiation that is detected at angle θ_t in the range $\theta_{\mathrm{ac}}^{(1)} < \theta_t < \pi/2$ originates from evanescent waves. From a different point of view, when angle θ_t is increased from zero, the angle of incidence also increases, up to the point where it reaches $\pi/2$. At this point, $\theta_t = \theta_{\mathrm{ac}}^{(1)}$, and a further increase of θ_t then yields a corresponding evanescent incident wave. This situation is exactly the opposite of total internal reflection, where the angle of incidence θ_{inc} reaches a critical value $\theta_c^{(1)}$, given by Eq. (2), beyond which the transmitted wave becomes evanescent. Therefore we call $\theta_{\mathrm{ac}}^{(1)}$ the *anti*-critical angle.

For detection in $z < -L$, the dependence on the distance h between the surface and the dipole is through the factor $\exp[-2h\,\mathrm{Im}(n_1^2 - n_3^2\sin^2\theta)^{1/2}]$ in Eq. (31). Since $\sin\theta = \sin\theta_t$, we see that this factor equals unity for $0 \leqslant \theta_t \leqslant \theta_{\mathrm{ac}}^{(1)}$, and therefore there is no h dependence in the radiation pattern. In this range the corresponding dipole waves are traveling. Since traveling waves have the same amplitude everywhere, the travel distance between the dipole and the surface is irrelevant. On the other hand, for $\theta_t > \theta_{\mathrm{ac}}^{(1)}$ this factor gives an exponential dependence on h, reflecting the fact that the corresponding evanescent dipole waves decay exponentially from some finite value at $z = H$ to zero in the negative z direction. As a result, the detected power for $\theta_t > \theta_{\mathrm{ac}}^{(1)}$ diminishes rapidly with increasing h. This is illustrated in Fig. 4, where $h = 4\pi$, and it is seen that almost no radiation appears in $\theta_t > \theta_{\mathrm{ac}}^{(1)}$.

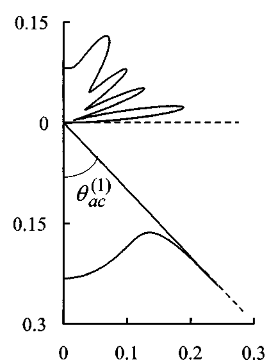

Fig. 4. Radiation pattern $A(\theta,\ \phi)$ for $n_1 = 1$, $n_2 = n_3 = 1.41$, $h = 4\pi$, and $\mathbf{u} = \mathbf{e}_1$. The anti-critical angle is $\theta_{\mathrm{ac}}^{(1)} = 45°$, indicated by the dashed line. The fraction of evanescent power for this case is $f = 0.56\%$.

7. POWER OF THE EVANESCENT WAVES

For the radiation in $z > H$ we have $0 \leqslant \theta < \pi/2$, and the corresponding range of α is $0 \leqslant \alpha < n_1$, because $\alpha = n_1 \sin \theta_{\text{inc}}$ and $\theta = \theta_{\text{inc}}$. This shows that exactly all traveling dipole waves contribute to the radiation in $z > H$, and there is no contribution from evanescent waves here. For detection in $z < -L$ the range of α is $0 \leqslant \alpha < n_3$, since $\alpha = n_3 \sin \theta_t$. If $n_3 < n_1$, the corresponding dipole waves are traveling, and there is no contribution from evanescent waves. For values of α in the range $n_3 < \alpha < n_1$, there are still traveling dipole waves incident on the surface $z = 0$, but the angle of incidence is larger than the critical angle $\theta_c^{(1)}$, Eq. (2), and therefore the transmitted waves in medium n_3 are evanescent, and they do not appear in the far field as radiation. Only for $n_3 > n_1$ can we have evanescent dipole waves appearing in the far field, in $z < -L$, which are converted by the layer into traveling waves.

In order to quantify the relative contribution of the evanescent waves to the power transmitted through the layer, we consider the integrated power. To this end, we first notice that the ϕ dependence of the intensity distribution $A(\theta, \phi)$ is purely geometrical since it enters only through the unit vectors $\mathbf{e}_\theta$, $\mathbf{e}_\phi$, and $\mathbf{e}_\rho$. The θ dependence, on the other hand, is essential, as follows from the fact that $\sin \theta$ appears in the arguments of the Fresnel coefficients. Another θ dependence enters through $\mathrm{d}\Omega = \sin \theta \mathrm{d}\theta \mathrm{d}\phi$. We therefore introduce

$$B(\theta) = \sin \theta \int_0^{2\pi} \mathrm{d}\phi A(\theta, \phi), \tag{33}$$

in terms of which the power per unit polar angle, emitted in the θ direction, becomes

$$\frac{\mathrm{d}P}{\mathrm{d}\theta} = P_o B(\theta). \tag{34}$$

Performing the integrations over ϕ then yields

$$\begin{aligned} B(\theta) = {} & \tfrac{3}{8} n_1 \sin \theta (1 - |u_z|^2) \\ & \times [|1 + R_s(n_1 \sin \theta) \exp(2 i n_1 h \cos \theta)|^2 \\ & + \cos^2 \theta |1 - R_p(n_1 \sin \theta) \exp(2 i n_1 h \cos \theta)|^2] \\ & + \tfrac{3}{4} n_1 \sin^3 \theta |u_z|^2 \\ & \times |1 + R_p(n_1 \sin \theta) \exp(2 i n_1 h \cos \theta)|^2, \end{aligned} \tag{35}$$

for $z > H$, and

$$\begin{aligned} B(\theta) = {} & \frac{3 n_3{}^3}{8 n_1{}^2} \frac{\sin \theta \cos^2 \theta}{|n_1{}^2 - n_3{}^2 \sin^2 \theta|} [(1 - |u_z|^2) \\ & \times (n_1{}^2 |T_s(n_3 \sin \theta)|^2 \\ & + |n_1{}^2 - n_3{}^2 \sin^2 \theta| |T_p(n_3 \sin \theta)|^2) \\ & + 2 |u_z|^2 n_3{}^2 \sin^2 \theta |T_p(n_3 \sin \theta)|^2] \\ & \times \exp[-2h \operatorname{Im}(n_1{}^2 - n_3{}^2 \sin^2 \theta)^{1/2}], \end{aligned} \tag{36}$$

for $z < -L$. It is interesting to notice that the dependence on the dipole orientation vector $\mathbf{u}$ enters only as $|u_z|^2$, with $0 \leqslant |u_z|^2 \leqslant 1$, in contrast to the result for $A(\theta, \phi)$, which depends on the three Cartesian components of $\mathbf{u}$ separately.

The transmitted power due to traveling dipole waves ends up in the cone $0 \leqslant \theta_t \leqslant \theta_{\text{ac}}^{(1)}$ and is given by

$$P_{\text{tr}} = P_o \int_{\pi - \theta_{\text{ac}}^{(1)}}^{\pi} \mathrm{d}\theta B(\theta), \tag{37}$$

whereas the contribution from evanescent waves is

$$P_{\text{ev}} = P_o \int_{\pi/2}^{\pi - \theta_{\text{ac}}^{(1)}} \mathrm{d}\theta B(\theta). \tag{38}$$

As a measure for the relative contribution of the evanescent waves, we define

$$f = \frac{P_{\text{ev}}}{P_{\text{ev}} + P_{\text{tr}}} \times 100\%. \tag{39}$$

The quantities P_{ev} and P_{tr} are computed by numerical integration. For parameters as in Fig. 4, with $h = 4\pi$, the value of f is found to be 0.56%, indicating that only a very small fraction of the power is due to evanescent waves in this case. An example of just the opposite situation is illustrated in Fig. 5, where $h = 0$. Here we find $f = 95\%$, and the figure clearly shows that nearly all intensity is emitted at a transmission angle larger than $\theta_{\text{ac}}^{(1)}$.

In order to illustrate the significance of the evanescent waves, we consider a single $n_1 - n_3$ interface (this affects only the Fresnel coefficients, which simplify considerably) and $h = 0$. Then it can be shown that P_{ev} and P_{tr} are functions of n_1/n_3 only, with both an overall factor of n_3. For a dipole embedded in a medium with index of refraction n_3, the total power emitted in all directions is $n_3 P_o$. Figure 6 shows $P_{\text{ev}}/(n_3 P_o)$, $P_{\text{tr}}/(n_3 P_o)$, and f as functions of n_1/n_3 for a dipole in the xy plane. Notice that the independent variable n_1/n_3 equals $\sin \theta_{\text{ac}}^{(1)}$. At approximately $n_1/n_3 \approx 0.8$, we have $P_{\text{ev}} = P_{\text{tr}}$, and for $n_3 > 1.25 n_1$ the power of the evanescent waves exceeds the power of the traveling waves. Figure 7 shows the

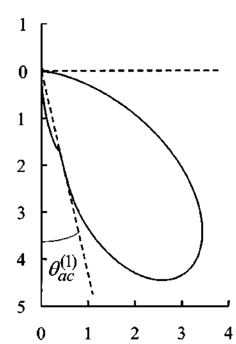

Fig. 5. Polar diagram of the intensity distribution $B(\theta)$ for $n_1 = 1$, $n_2 = n_3 = 4.47$, for which $\theta_{\text{ac}}^{(1)} = 30°$, and $h = 0$. The dipole unit vector here is $\mathbf{u} = \mathbf{e}_z$, and $f = 95\%$. We see that almost all power in $z < -L$ comes from evanescent waves, and it is interesting to notice that the emission of traveling waves in $z > H$ is negligible.

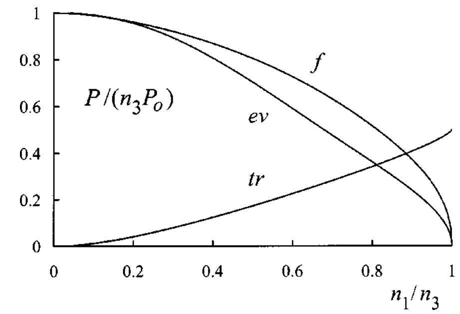

Fig. 6. Graphs of $P_{\mathrm{tr}}/(n_3P_o)$, $P_{\mathrm{ev}}/(n_3P_o)$ and the corresponding fraction f, as a function of n_1/n_3 for a dipole along the z axis.

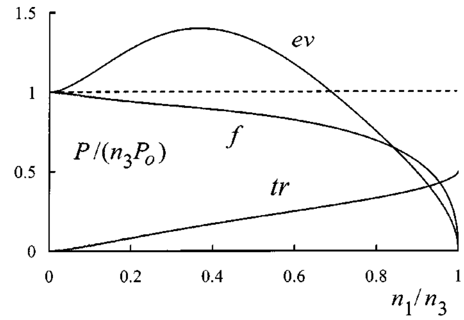

Fig. 7. Same as Fig. 6 but for a dipole in the xy plane. Of interest here is that the evanescent power can exceed the power of a free dipole in medium n_3.

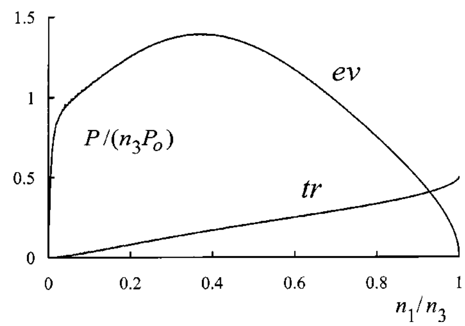

Fig. 8. Same as Fig. 7 but for $h = 0.00314$. Already for this small value of h, we see that $P_{\mathrm{ev}}/(n_3P_o)$ falls to zero for $n_1/n_3 \to 0$.

same graphs for a dipole along the z axis. Here we see that for almost all values of n_1/n_3 the evanescent waves dominate. Moreover, there is a large region where $P_{\mathrm{ev}}/(n_3P_o) > 1$; e.g., the power of the evanescent waves alone is larger than the total power that would be emitted by a dipole in medium n_3 and without any interface.

For the case of a single interface and $h = 0$, the value of P_{ev} can be obtained in closed form. Evaluating the integral in Eq. (38) yields

$$P_{\mathrm{ev}}/(n_3P_o) = \frac{1}{2\sqrt{1-r}}\frac{1}{(1+r)^2}\{(1-|u_z|^2) \times [3-(1-r^2)(1-r)-r\,\eta(r)] + 2|u_z|^2[1-r^2-3r+\eta(r)]\}, \quad (40)$$

where $r = n_1{}^2/n_3{}^3$, and the function $\eta(r)$ is defined as

$$\eta(r) = \frac{3r}{\sqrt{1-r^2}}\ln\left(\frac{1+\sqrt{1-r^2}}{r}\right). \quad (41)$$

For $n_3 \gg n_1$ we have $r \to 0$, and with $\eta(0) = 0$ this gives $P_{\mathrm{ev}} = n_3P_o$, showing that for a dense medium n_3, relative to n_1, the power of the evanescent waves is the same as the power of a free dipole in medium n_3, for which all waves are traveling. It should be noted that this conclusion strictly holds for $h = 0$ only. The h dependence of $B(\theta)$ in Eq. (36) comes in through the factor $\exp[-2h\,\mathrm{Im}(n_1{}^2 - n_3{}^2\sin^2\theta)^{1/2}]$, which can also be written as $\exp[-2hn_3\,\mathrm{Im}(\sin^2\theta_{\mathrm{ac}}^{(1)} - \sin^2\theta_t)^{1/2}]$. Since $\sin\theta_{\mathrm{ac}}^{(1)} < \sin\theta$ for $\theta_{\mathrm{ac}}^{(1)} < \theta_t < \pi/2$, the exponent is nonzero; and for any finite h, an increasing n_3 makes this factor vanish. Therefore $P_{\mathrm{ev}}/(n_3P_o) \to 0$ for $h \neq 0$ and $r \to 0$. This feature is illustrated in Fig. 8.

8. ANTI-CRITICAL ANGLE OF THE SECOND KIND

The anti-critical angle of the first kind is the transmission angle at which the incident wave turns evanescent. We now consider the waves in the layer with index of refraction n_2. When these are traveling waves with angle θ_2 with respect to the normal, then we have $\sin\theta_2 = (n_3/n_2)\sin\theta_t$, given θ_t. When $n_3 > n_2$, θ_2 reaches $\pi/2$ at the transmission angle $\theta_{\mathrm{ac}}^{(2)}$ given by

$$\sin\theta_{\mathrm{ac}}^{(2)} = n_2/n_3. \quad (42)$$

Then for $\theta_{\mathrm{ac}}^{(2)} < \theta_t < \pi/2$ the waves in the layer are evanescent, which greatly reduces the transmission with increasing L. It should be noted that this phenomenon is independent of the nature of the incident dipole waves. Also, we can have two anti-critical angles, with either $\theta_{\mathrm{ac}}^{(1)} < \theta_{\mathrm{ac}}^{(2)}$ or $\theta_{\mathrm{ac}}^{(1)} > \theta_{\mathrm{ac}}^{(2)}$, or we can have only $\theta_{\mathrm{ac}}^{(1)}$ or only $\theta_{\mathrm{ac}}^{(2)}$, or none at all, depending on the relative values of n_1, n_2 and n_3.

Figure 9 shows the effect of the second anti-critical angle for the case of $\theta_{\mathrm{ac}}^{(1)} < \theta_{\mathrm{ac}}^{(2)}$. For $0 \leqslant \theta_t < \theta_{\mathrm{ac}}^{(1)}$, the dipole, layer and transmitted waves are all traveling. For $\theta_{\mathrm{ac}}^{(1)} < \theta_t < \theta_{\mathrm{ac}}^{(2)}$, the dipole waves are evanescent but the waves in the layer are still traveling, and for $\theta_{\mathrm{ac}}^{(2)} < \theta_t < \pi/2$ both the dipole and the layer waves are eva-

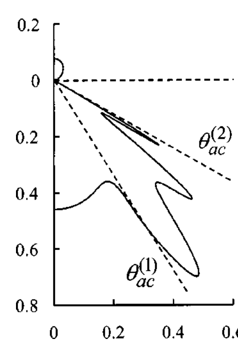

Fig. 9. Graph of the intensity distribution $A(\theta, \phi)$, illustrating the effect of the second critical angle $\theta_{\mathrm{ac}}^{(2)}$. The parameters are $n_1 = 1$, $n_2 = 1.73$, $n_3 = 2$, $h = 0$, $l = 2\pi$ and $\mathbf{u} = \mathbf{e}_1$. Here we have $\theta_{\mathrm{ac}}^{(1)} = 30°$, $\theta_{\mathrm{ac}}^{(2)} = 60°$, and $f = 75\%$. We see that owing to the layer thickness, almost no power is emitted in the range $\theta_{\mathrm{ac}}^{(2)} < \theta_{\mathrm{t}} < \pi/2$.

nescent, with, of course, the transmitted waves still traveling. In Fig. 9 we have $l = 2\pi$, with $l = k_o L$ the dimensionless layer thickness, so we have a layer thickness of one wavelength of the incident radiation ($n_1 = 1$). We see that the transmission in $\theta_{ac}^{(2)} < \theta_t < \pi/2$ has already become negligible for this relatively small value of l. It is interesting to notice that in the region $\theta_{ac}^{(1)} < \theta_t < \theta_{ac}^{(2)}$ there seems to be an interference structure. This cannot be the case, however, because for a given angle θ_t there is only a single wave, according to the stationary-phase interpretation. From Eqs. (A5) and (A6) we see that the Fresnel transmission coefficients have a factor of $\exp(2i\nu_2\ell)$ in the denominator. This can also be written as $\exp[2in_3\ell(\sin^2\theta_{ac}^{(2)} - \sin^2\theta_t)^{1/2}]$. For $\theta_t < \theta_{ac}^{(2)}$, the exponent is imaginary, leading to oscillations with varying θ_t. This, of course, is a reflection of the interference of the waves with wave vectors $\mathbf{k}_-$ and $\mathbf{k}_+$, representing the traveling waves in the layer [Fig. 2(a)], and this affects the Fresnel transmission coefficients.

9. CONCLUSIONS

Dipole radiation is a superposition of traveling and evanescent plane waves when represented by an angular spectrum. For a dipole embedded in a medium with index of refraction n_1, only the traveling waves contribute to the radiation in the far field, and the evanescent waves remain unobserved. When the radiation passes through an interface or a layer, as in Fig. 1, a portion of the evanescent waves will be converted into traveling waves if $n_3 > n_1$, and they become observable in the far field. We have shown that there exists a transmission angle $\theta_{ac}^{(1)}$ that has the significance that any radiation detected in $\theta_{ac}^{(1)} < \theta_t < \pi/2$ has its origin in evanescent dipole waves. Partial angular spectrum waves with their $\mathbf{k}_\parallel$ vector in the ring $k_o n_1 < k_\parallel < k_o n_3$ in the $\mathbf{k}_\parallel$ plane contribute to this phenomenon, and the observation direction $\hat{\mathbf{r}}$ of the emanating traveling wave determines uniquely the corresponding $\mathbf{k}_\parallel$ in this ring. In this fashion, the evanescent field of the dipole can be partially observed in the far field, and this has been seen experimentally.[18] In more-contemporary measurements, the sample is placed in air or in an aqueous solution with low index of refraction on an oil-immersion hemispherical lens. In this geometry, the radiation in the far field exits the lens under normal incidence, and the intensity distribution should greatly resemble the results presented in this paper for $z < 0$.

We have also shown that the total power in the far field due to evanescent dipole waves can greatly exceed the contribution of the traveling waves ($f = 95\%$ in Fig. 5) and that this power can exceed the power by a free dipole in medium n_3. Finally, when transmission through a layer is considered, a second anti-critical transmission angle $\theta_{ac}^{(2)}$ appears when $n_3 > n_2$. For $\theta_t > \theta_{ac}^{(2)}$, the waves in the layer become evanescent, and hardly any radiation will appear in this region of observation when the layer thickness L is not too small.

APPENDIX A

The Fresnel reflection and transmission coefficients depend on the three indices of refraction, the dimensionless layer thickness $\ell = k_o L$, and the variable α, representing in dimensionless form the value of $k_\parallel$. These Fresnel coefficients are most conveniently expressed in terms of the three v_i from Eq. (7). With the notation

$$\Lambda_s = (\nu_1 + \nu_2)(\nu_2 + \nu_3) + (\nu_1 - \nu_2)(\nu_2 - \nu_3) \times \exp(2i\nu_2\ell), \tag{A1}$$

$$\Lambda_p = (n_2{}^2\nu_1 + n_1{}^2\nu_2)(n_3{}^2\nu_2 + n_2{}^2\nu_3) + (n_2{}^2\nu_1 - n_1{}^2\nu_2)(n_3{}^2\nu_2 - n_2{}^2\nu_3)\exp(2i\nu_2\ell), \tag{A2}$$

we have

$$R_s(\alpha) = \frac{1}{\Lambda_s}[(\nu_1 - \nu_2)(\nu_2 + \nu_3) + (\nu_1 + \nu_2)(\nu_2 - \nu_3) \times \exp(2i\nu_2\ell)], \tag{A3}$$

$$R_p(\alpha) = \frac{1}{\Lambda_p}[(n_2{}^2\nu_1 - n_1{}^2\nu_2)(n_3{}^2\nu_2 + n_2{}^2\nu_3) + (n_2{}^2\nu_1 + n_1{}^2\nu_2)(n_3{}^2\nu_2 - n_2{}^2\nu_3)\exp(2i\nu_2\ell)], \tag{A4}$$

$$T_s(\alpha) = \frac{4\nu_1\nu_2}{\Lambda_s}\exp[i(\nu_2 - \nu_3)\ell], \tag{A5}$$

$$T_p(\alpha) = \frac{4\nu_1\nu_2 n_1 n_2{}^2 n_3}{\Lambda_p}\exp[i(\nu_2 - \nu_3)\ell]. \tag{A6}$$

The authors' e-mail addresses are arnoldus @ra.msstate.edu and jtf1@ra.msstate.edu.

REFERENCES

1. D. W. Pohl, "Scanning near-field optical microscopy," in *Advances in Optical and Electron Microscopy*, T. Mulvey and C. J. R. Sheppard, eds. (Academic, San Diego, Calif., 1991), p. 243.
2. D. W. Pohl and D. Courjon, (eds.,) *Near Field Optics*, Proceedings of the NATO Advanced Research Workshop on Near Field Optics, Series E, Applied Sciences, Vol. 242 (Kluwer, Dordrecht, The Netherlands, 1993).
3. D. Courjon and C. Bainier, "Near field microscopy and near field optics," Rep. Prog. Phys. **57**, 989–1028 (1994).
4. M. A. Paesler and P. J. Moyer, *Near Field Optics, Theory, Instrumentation, and Applications* (Wiley, New York, 1996).
5. M. Ohtsu, ed., *Near-Field Nano/Atom Optics and Technology* (Springer, Berlin, 1998).
6. K. T. V. Grattan and B. T. Meggitt, eds., *Optical Fiber Sensor Technology, Fundamentals* (Kluwer, Dordrecht, The Netherlands, 2000).
7. D. Courjon, *Near-Field Microscopy and Near-Field Optics* (World Scientific, Singapore, 2003).
8. L. Novotny, D. W. Pohl, and P. Regli, "Light propagation through nanometer-sized structures: the two-dimensional-aperture scanning near-field optical microscope," J. Opt. Soc. Am. A **11**, 1768–1779 (1994).
9. H. Heinzelmann, B. Hecht, L. Novotny, and D. W. Pohl, "Forbidden light scanning near-field optical microscopy," J. Microsc. **177**, 115–118 (1995).
10. D. Van Labeke, F. Baida, D. Barchiesi, and D. Courjon, "A theoretical model for the inverse scanning tunneling optical microscope (ISTOM)," Opt. Commun. **114**, 470–480 (1995).
11. G. A. Massey, "Microscopy and pattern generation with scanned evanescent waves," Appl. Opt. **23**, 658–660 (1984).
12. J. M. Vigoureux, F. Depasse, and C. Girard, "Superresolu-

tion of near-field optical microscopy defined from properties of confined electromagnetic waves," Appl. Opt. **31**, 3036–3045 (1992).

13. D. Van Labeke, D. Barchiesi, and F. Baida, "Optical characterization of nanosources used in scanning near-field optical microscopy," J. Opt. Soc. Am. A **12**, 695–703 (1995).
14. B. Hecht, D. W. Pohl, and H. Heinzelmann, "Tunnel near-field optical microscopy: TNOM-2," in *Photons and Local Probes*, O. Marti and R. Möller, eds. (Kluwer, Dordrecht, The Netherlands, 1995), p. 93–107.
15. B. Hecht, H. Bielefeldt, and D. W. Pohl, "Influence of detection conditions on near-field optical imaging," J. Appl. Phys. **84**, 5873–5882 (1998).
16. B. Hecht, "Forbidden light scanning near-field optical microscopy," doctoral thesis (University of Basel, Basel, Switzerland, 1996).
17. H. F. Arnoldus and J. T. Foley, "Spatial separation of the traveling and evanescent parts of dipole radiation," Opt. Lett. **28**, 1299–1301 (2003).
18. C. K. Carniglia, L. Mandel, and K. H. Drexhage, "Absorption and emission of evanescent photons," J. Opt. Soc. Am. **62**, 479–486 (1972).
19. L. Mandel and E. Wolf, *Optical Coherence and Quantum Optics* (Cambridge U. Press, Cambridge, UK, 1995), Sec. 3.2.4.
20. O. Keller, "Screened electromagnetic propagators in nonlocal metal optics," Phys. Rev. B **34**, 3883–3899 (1986).
21. H. F. Arnoldus and J. T. Foley, "Traveling and evanescent parts of the optical near field," J. Mod. Opt. **50**, 1883–1901 (2003).
22. J. E. Sipe, "The dipole antenna problem in surface physics: a new approach," Surf. Sci. **105**, 489–504 (1981).
23. J. E. Sipe, "New Green function formalism for surface optics," J. Opt. Soc. Am. B **4**, 481–489 (1987).
24. M. Born and E. Wolf, *Principles of Optics*, 7th (expanded) ed. (Cambridge U. Press, Cambridge, UK, 1999), App. III, p. 890.
25. G. C. Sherman, J. J. Stamnes, and É. Lalor, "Asymptotic approximations to angular-spectrum representations," J. Math. Phys. **17**, 760–776 (1976).
26. J. Gasper, G. C. Sherman, and J. J. Stamnes, "Reflection and refraction of an arbitrary electromagnetic wave at a plane interface," J. Opt. Soc. Am. **66**, 955–961 (1976).
27. J. D. Jackson, *Classical Electrodynamics*, 2nd ed. (Wiley, New York, 1975), p. 396.
28. K. H. Drexhage, "Interaction of light with monomolecular dye layers," Prog. Opt. **XII**, 163–232 (1974).
29. W. Lukosz and R. E. Kunz, "Light emission by magnetic and electric dipoles close to a plane interface. I. Total radiated power," J. Opt. Soc. Am. **67**, 1607–1615 (1977).
30. W. Lukosz and R. E. Kunz, "Light emission by magnetic and electric dipoles close to a plane interface. II. Radiation patterns of perpendicular oriented dipoles," J. Opt. Soc. Am. **67**, 1615–1619 (1977).
31. W. Lukosz, "Theory of optical-environment-dependent spontaneous-emission rates for emitters in thin layers," Phys. Rev. B **22**, 3030–3038 (1980).